Generation of 64 GBd 4ASK signals using a silicon-organic hybrid modulator at 80 °C

M. Lauermann,[1] S. Wolf,[1] W. Hartmann,[1] R. Palmer,[1,5] Y. Kutuvantavida,[1] H. Zwickel,[1] A. Bielik,[2] L. Altenhain,[2] J. Lutz,[2] R. Schmid,[2] T. Wahlbrink,[3] J. Bolten,[3] A. L. Giesecke,[3] W. Freude,[1] and C. Koos[1,4,*]

[1]*Karlsruhe Institute of Technology, Institute of Photonics and Quantum Electronics, 76133 Karlsruhe, Germany*
[2]*Micram Microelectronic GmbH, 44801 Bochum, Germany*
[3]*AMO GmbH, 52074 Aachen, Germany*
[4]*Karlsruhe Institute of Technology, Institute of Microstructure Technology, 76344 Eggenstein-Leopoldshafen, Germany*
[5]*Now with Coriant GmbH, 81541 Munich, Germany*
[*]*christian.koos@kit.edu*

Abstract: We demonstrate a silicon-organic hybrid (SOH) Mach-Zehnder modulator (MZM) generating four-level amplitude shift keying (4ASK) signals at symbol rates of up to 64 GBd both at room temperature and at an elevated temperature of 80 °C. The measured line rate of 128 Gbit/s corresponds to the highest value demonstrated for silicon-based MZM so far. We report bit error ratios of 10^{-10} (64 GBd BPSK), 10^{-5} (36 GBd 4ASK), and 4×10^{-3} (64 GBd 4ASK) at room temperature. At 80 °C, the respective bit error ratios are 10^{-10}, 10^{-4}, and 1.3×10^{-2}. The high-temperature experiments were performed in regular oxygen-rich ambient atmosphere.

OCIS codes: (060.4080) Modulation; (250.7360) Waveguide modulators; (250.5300) Photonic integrated circuits.

References and links

1. M. Hochberg, N. C. Harris, R. Ding, Y. Zhang, A. Novack, Z. Xuan, and T. Baehr-Jones, "Silicon photonics: The next fabless semiconductor industry," IEEE Solid State Circ. Mag. **5**(1), 48–58 (2013).
2. J. S. Orcutt, B. Moss, C. Sun, J. Leu, M. Georgas, J. Shainline, E. Zgraggen, H. Li, J. Sun, M. Weaver, S. Urošević, M. Popović, R. J. Ram, and V. Stojanović, "Open foundry platform for high-performance electronic-photonic integration," Opt. Express **20**(11), 12222–12232 (2012).
3. G. T. Reed, G. Mashanovich, F. Y. Gardes, and D. J. Thomson, "Silicon optical modulators," Nat. Photonics **4**(8), 518–526 (2010).
4. B. Milivojevic, C. Raabe, A. Shastri, M. Webster, P. Metz, S. Sunder, B. Chattin, S. Wiese, B. Dama, and K. Shastri, "112Gb/s DP-QPSK transmission over 2427km SSMF using small-size silicon photonic IQ modulator and low-power CMOS driver," in *Optical Fiber Communication Conference, 2013* (OSA, 2013), p. OTh1D.1.
5. M. R. Watts, W. A. Zortman, D. C. Trotter, R. W. Young, and A. L. Lentine, "Low-voltage, compact, depletion-mode, silicon Mach-Zehnder modulator," IEEE J. Sel. Top. Quantum Electron. **16**(1), 159–164 (2010).
6. P. Dong, X. Liu, S. Chandrasekhar, L. L. Buhl, R. Aroca, and Y.-K. Chen, "Monolithic silicon photonic integrated circuits for compact 100+ Gb/s coherent optical receivers and transmitters," IEEE J. Sel. Top. Quantum Electron. **20**, 1–8 (2014).
7. H. Xu, X. Li, X. Xiao, P. Zhou, Z. Li, J. Yu, and Y. Yu, "High-speed silicon modulator with band equalization," Opt. Lett. **39**(16), 4839–4842 (2014).
8. P. Dong, C. Xie, L. L. Buhl, Y.-K. Chen, J. H. Sinsky, and G. Raybon, "Silicon in-phase/quadrature modulator with on-chip optical equalizer," in *40th European Conference on Optical Communication (ECOC 2014)* (2014), p. We.1.4.5.
9. J. Geyer, C. R. Doerr, M. Aydinlik, N. Nadarajah, A. Caballero, C. Rasmussen, and B. Mikkelsen, "Practical implementation of higher order modulation beyond 16-QAM," in *Optical Fiber Communication Conference 2015* (OSA, 2015), p. Th1B.1.
10. Y. Fang, L. Liu, C. Y. Wong, S. Zhang, T. Wang, G. N. Liu, and X. Xu, "Silicon IQ modulator based 480km 80x453.2Gb/s PDM-eOFDM transmission on 50GHz grid with SSMF and EDFA-only link," in *Opt. Fiber Commun. Conf. 2015* (OSA, 2015), p. M3G.5.
11. T. Baehr-Jones, M. Hochberg, G. Wang, R. Lawson, Y. Liao, P. Sullivan, L. Dalton, A. Jen, and A. Scherer, "Optical modulation and detection in slotted silicon waveguides," Opt. Express **13**(14), 5216–5226 (2005).

#258670 Received 2 Feb 2016; revised 5 Mar 2016; accepted 11 Mar 2016; published 20 Apr 2016

12. C. Koos, J. Brosi, M. Waldow, W. Freude, and J. Leuthold, "Silicon-on-insulator modulators for next-generation 100 Gbit/s-ethernet," in *33rd European Conference and Exhibition of Optical Communication (ECOC)* (VDE, 2007).
13. C. Koos, J. Leuthold, W. Freude, M. Kohl, L. Dalton, W. Bogaerts, A. Giesecke, M. Lauermann, A. Melikyan, S. Koeber, S. Wolf, C. Weimann, S. Muehlbrandt, K. Koehnle, J. Pfeifle, W. Hartmann, Y. Kutuvantavida, S. Ummethala, R. Palmer, D. Korn, L. Alloatti, P. Schindler, D. Elder, T. Wahlbrink, and J. Bolten, "Silicon-organic hybrid (SOH) and plasmonic-organic hybrid (POH) integration," J. Lightwave Technol. **34**(2), 256–268 (2016).
14. R. Palmer, S. Koeber, D. Elder, M. Woessner, W. Heni, D. Korn, M. Lauermann, W. Bogaerts, L. Dalton, W. Freude, J. Leuthold, and C. Koos, "High-speed, low drive-voltage silicon-organic hybrid modulator based on a binary-chromophore electro-optic material," J. Lightwave Technol. **32**(16), 2726–2734 (2014).
15. S. Koeber, R. Palmer, M. Lauermann, W. Heni, D. L. Elder, D. Korn, M. Woessner, L. Alloatti, S. Koenig, P. C. Schindler, H. Yu, W. Bogaerts, L. R. Dalton, W. Freude, J. Leuthold, and C. Koos, "Femtojoule electro-optic modulation using a silicon–organic hybrid device," Light Sci. Appl. **4**(2), e255 (2015).
16. W. Hartmann, M. Lauermann, S. Wolf, H. Zwickel, Y. Kutuvantavida, J. Luo, A. K.-Y. Jen, W. Freude, and C. Koos, "100 Gbit/s OOK using a silicon-organic hybrid (SOH) modulator," in *European Conference on Optical Communication (ECOC), 2015* (IEEE, 2015), p. PDP.1.4.
17. M. Lauermann, R. Palmer, S. Koeber, P. C. Schindler, D. Korn, T. Wahlbrink, J. Bolten, M. Waldow, D. L. Elder, L. R. Dalton, J. Leuthold, W. Freude, and C. Koos, "Low-power silicon-organic hybrid (SOH) modulators for advanced modulation formats," Opt. Express **22**(24), 29927–29936 (2014).
18. M. Lauermann, S. Wolf, P. C. Schindler, R. Palmer, S. Koeber, D. Korn, L. Alloatti, T. Wahlbrink, J. Bolten, M. Waldow, M. Koenigsmann, M. Kohler, D. Malsam, D. L. Elder, P. V. Johnston, N. Phillips-Sylvain, P. A. Sullivan, L. R. Dalton, J. Leuthold, W. Freude, and C. Koos, "40 GBd 16QAM signaling at 160 Gb/s in a silicon-organic hybrid modulator," J. Lightwave Technol. **33**(6), 1210–1216 (2015).
19. S. Wolf, M. Lauermann, P. Schindler, G. Ronniger, K. Geistert, R. Palmer, S. Kober, W. Bogaerts, J. Leuthold, W. Freude, and C. Koos, "DAC-less amplifier-less generation and transmission of QAM signals using sub-volt silicon-organic hybrid modulators," J. Lightwave Technol. **33**(7), 1425–1432 (2015).
20. S. Huang, J. Luo, Z. Jin, X.-H. Zhou, Z. Shi, and A. K.-Y. Jen, "Enhanced temporal stability of a highly efficient guest–host electro-optic polymer through a barrier layer assisted poling process," J. Mater. Chem. **22**(38), 20353 (2012).
21. M. Lauermann, S. Wolf, R. Palmer, A. Bielik, L. Altenhain, J. Lutz, R. Schmid, T. Wahlbrink, J. Bolten, A. L. Giesecke, W. Freude, and C. Koos, "64 GBd operation of a silicon-organic hybrid modulator at elevated temperature," in *Optical Fiber Communication Conference, 2015* (OSA, 2015), p. Tu2A.5.
22. J. Witzens, T. Baehr-Jones, and M. Hochberg, "Design of transmission line driven slot waveguide Mach-Zehnder interferometers and application to analog optical links," Opt. Express **18**(16), 16902–16928 (2010).
23. L. Alloatti, M. Lauermann, C. Sürgers, C. Koos, W. Freude, and J. Leuthold, "Optical absorption in silicon layers in the presence of charge inversion/accumulation or ion implantation," Appl. Phys. Lett. **103**(5), 051104 (2013).
24. L. Alloatti, R. Palmer, S. Diebold, K. P. Pahl, B. Chen, R. Dinu, M. Fournier, J.-M. Fedeli, T. Zwick, W. Freude, C. Koos, and J. Leuthold, "100 GHz silicon–organic hybrid modulator," Light Sci. Appl. **3**(5), e173 (2014).
25. R. Palmer, L. Alloatti, D. Korn, W. Heni, P. C. Schindler, J. Bolten, M. Karl, M. Waldow, T. Wahlbrink, W. Freude, C. Koos, and J. Leuthold, "Low-loss silicon strip-to-slot mode converters," IEEE Photonics J. **5**(1), 2200409 (2013).
26. R. Soref and B. Bennett, "Electrooptical effects in silicon," IEEE J. Quantum Electron. **23**(1), 123–129 (1987).
27. R. Ding, T. Baehr-Jones, W.-J. Kim, X. Xiong, R. Bojko, J.-M. Fedeli, M. Fournier, and M. Hochberg, "Low-loss strip-loaded slot waveguides in sSilicon-on-insulator," Opt. Express **18**(24), 25061–25067 (2010).
28. R. Schmogrow, B. Nebendahl, M. Winter, A. Josten, D. Hillerkuss, S. Koenig, J. Meyer, M. Dreschmann, M. Huebner, C. Koos, J. Becker, W. Freude, and J. Leuthold, "Error vector magnitude as a performance measure for advanced modulation formats," IEEE Photon. Technol. Lett. **24**, 61–63 (2012). [Correction: ibid., **24**, 2198 (2012)].
29. Z. Shi, J. Luo, S. Huang, B. M. Polishak, X.-H. Zhou, S. Liff, T. R. Younkin, B. A. Block, and A. K.-Y. Jen, "Achieving excellent electro-optic activity and thermal stability in poled polymers through an expeditious crosslinking process," J. Mater. Chem. **22**(3), 951–959 (2012).
30. F. Chang, K. Onohara, and T. Mizuochi, "Forward error correction for 100 G transport networks," IEEE Commun. Mag. **48**(3), S48–S55 (2010).
31. D. Chang, F. Yu, Z. Xiao, Y. Li, N. Stojanovic, C. Xie, X. Shi, X. Xu, and Q. Xiong, "FPGA verification of a single QC-LDPC code for 100 Gb/s optical systems without error floor down to BER of 10^{-15}," in *Optical Fiber Communication Conference (OFC)* (OSA, 2011), p. OTuN2.
32. L. R. Dalton, P. A. Sullivan, and D. H. Bale, "Electric field poled organic electro-optic materials: state of the art and future prospects," Chem. Rev. **110**(1), 25–55 (2010).
33. J. Luo, S. Huang, Z. Shi, B. M. Polishak, X.-H. Zhou, and A. K. Jen, "Tailored organic electro-optic materials and their hybrid systems for device applications," Chem. Mater. **23**(3), 544–553 (2011).

1. Introduction

Power-efficient photonic-electronic interfaces operating at high speed are key elements of high-performance data and telecommunication networks. With the widespread adoption of

#258670 Received 2 Feb 2016; revised 5 Mar 2016; accepted 11 Mar 2016; published 20 Apr 2016

coherent transmission techniques, Mach-Zehnder modulators (MZM) and MZM-based in-phase/quadrature (IQ) modulators have become central building blocks of such interfaces. To support advanced modulation formats, MZM must be capable of reliably generating multilevel signals at high symbol rate, low energy consumption, small footprint and low cost. Silicon photonics is an especially attractive integration platform for such devices: The high refractive index contrast of silicon-on-insulator (SOI) waveguides allows for compact devices and high integration density, while mature CMOS processing enables fabless mass production and opens a path towards large-scale co-integration with electronics [1,2]. Since the intrinsic inversion symmetry of the silicon crystal lattice prohibits any technically relevant second-order nonlinearities, current high-speed silicon MZM have to rely on carrier injection or depletion in reverse-biased *p-n* junctions that are integrated into the waveguide core [3,4]. This leads to rather low modulation efficiencies with minimum voltage-length products of the order of $U_\pi L = 10$ Vmm [5] and results in comparatively large, millimeter-long modulators which still require high drive voltages of up to 5 V [6]. For simple on-off-keying (OOK), the highest data rate demonstrated with an all-silicon MZM so far amounts to 70 Gbit/s [7]. Using advanced modulation formats, the highest symbol rates amount to 56 GBd, achieved in a QPSK signaling experiment with a line rate of 112 Gbit/s per polarization at a bit error ratio of 1×10^{-2} [8]. Higher line rates of up to 180 Gbit/s per polarization have been achieved by using more complex modulation formats such as 64QAM at symbol rates of 30 GBd [9], or by using electrical OFDM [10], but these implementations need extensive and power-hungry pre- and post-processing in the electrical domain to compensate for the impairments caused by the modulators' amplitude-phase coupling. The limitations of conventional all-silicon modulators can be overcome by silicon-organic hybrid (SOH) integration, which exploits organic electro-optic (EO) materials in combination with conventional SOI slot waveguides to realize pure phase modulators that do not suffer from amplitude-phase coupling [11–13]. With this approach, devices with significantly reduced voltage-length products of only $U_\pi L = 0.5$ Vmm have been demonstrated, enabling modulation at record-low energy consumption of only 1.6 fJ/bit [14,15]. In transmission experiments, SOH MZM have been demonstrated to enable data rates of 100 Gbit/s using simple OOK [16]. Similarly, SOH IQ modulators are perfectly suited for signaling with higher-order modulation formats such as 16QAM [17]. Symbol rates of up to 40 GBd and line rates of up 160 Gbit/s have been demonstrated experimentally [18]. The high efficiency of SOH devices even enables direct interfacing of IQ modulators to the binary outputs of an FPGA to generate 16QAM data streams without using preamplifiers or digital-to-analog converters [19]. However, while SOH modulators show great promise to further increase both symbol and data rates, the wider use of these devices is still hampered by doubts as to the temperature stability of the organic materials, in particular regarding the decay of acentric order in the poled material when operated at elevates temperatures.

In this paper we demonstrate that SOH Mach-Zehnder modulators can generate multi-level signals at symbol rates of up to 64 GBd, both at room temperature and at elevated temperatures of 80 °C. The high-temperature experiments were performed in regular oxygen-rich ambient atmosphere using an EO material, which is specified to be stable up a temperature of 85 °C [20]. In the experiment, we generate both binary phase shift keying (BPSK) and 4-level amplitude shift keying (4ASK) signals with a single 750 µm long SOH Mach-Zehnder modulator [21], achieving line rates of up to 128 Gbit/s. Our experiments represent the first demonstration of SOH devices operating at an elevated temperature, while achieving the highest data rate so far demonstrated for a silicon-based MZM.

2. Silicon-organic hybrid modulator

Silicon-organic hybrid modulators rely on the interaction of the light guided by an SOI waveguide with an EO cladding material which is exposed to an externally applied electric field [13]. Figure 1(a) shows a schematic (top) and a cross section of the SOH Mach-Zehnder modulator (MZM): Standard SOI strip waveguides form the interferometer together with multimode interference couplers (MMI) operating as amplitude splitter and combiner. In each

#258670 Received 2 Feb 2016; revised 5 Mar 2016; accepted 11 Mar 2016; published 20 Apr 2016

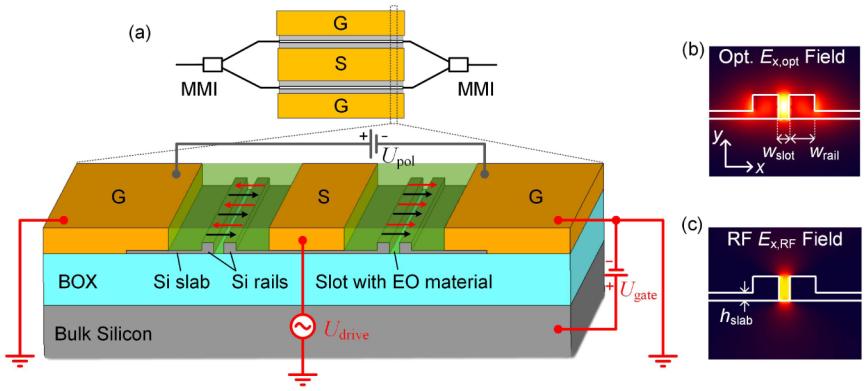

Fig. 1. Concept of the silicon-organic hybrid (SOH) modulator. (a) Schematic and cross-section of a silicon-organic hybrid (SOH) Mach-Zehnder modulator (MZM). Standard silicon strip waveguides and multimode interference coupler (MMI) form the waveguide interferometer. The phase shifter in each arm are based on a slot waveguide (rail width $w_{rail} = 240$ nm, slot width $w_{slot} = 120$ nm). A coplanar ground-signal-ground (GSG) RF transmission line carries the modulation signal and is electrically connected to the slot via *n*-doped silicon slabs (thickness $h_{slab} = 70$ nm). A gate voltage U_{Gate} between the Si substrate and the SOI device layer can be used to improve the conductivity of the silicon slab by electron accumulation at the slab-BOX interface, and hence increases the bandwidth of the device. The commercially available electro-optic (EO) organic material SEO100 from Soluxra, specified for an operating temperature of up to 85 °C, is deposited on the chip via spin coating, and serves as a nonlinear cladding. A poling voltage U_{pol} applied to the floating ground electrodes (G) aligns the chromophores (black arrows) when heating the EO material to its glass transition temperature close to 140 °C. After cooling, the orientation of the chromophores remains fixed. A modulating RF field (red arrows) applied to the GSG line results in push-pull operation of the phase modulator sections. (b) Distribution of the dominant electric field component $E_{x,opt}$ of the fundamental quasi-TE mode of the slot waveguide. (c) The electrical modulation field component $E_{x,RF}$ is strongly confined to the slot. The good overlap of optical and modulating fields results in an efficient modulation.

arm, the phase modulators are realized by SOI slot waveguides, the cross-section and the profile of the dominant optical electric field amplitude of which are shown in Fig. 1(b). The silicon rails and the slot have a width of $w_{rail} = 240$ nm and $w_{slot} = 120$ nm, respectively. The rails are connected to a coplanar ground-signal-ground (GSG) transmission line, Fig. 1(a), via conductive, slightly *n*-doped silicon slabs with a height of $h_{slab} = 70$ nm, Fig. 1(c). For the fundamental quasi-TE mode, the high refractive-index contrast between waveguide and EO cladding leads to an enhancement of the optical field within the slot, while a voltage applied to the transmission line drops mainly across the narrow slot leading a high modulation radio frequency (RF) field. Both fields overlap strongly, leading to an efficient modulation, see Fig. 1(b) for a contour plot of the dominant component of the optical mode ($E_{x,opt}$) and Fig. 1(c) for a plot of the $E_{x,RF}$ component of the modulation field. Due to the high modulation efficiency, the MZM can be as short as 750 µm. The transmission line of the modulator is designed for a characteristic impedance of 50 Ω, matched [17,22] to the characteristic impedance of common RF equipment. The bandwidth of the SOH device is typically limited by the RC time constant formed by the slot capacitance and the finite conductivity of the resistive slabs. To increase the slab conductivity, a gate voltage U_{gate} can be applied between the silicon substrate and the device layer to accumulate electrons at the interface between Si slabs and buried oxide (BOX), see Fig. 1(a) [23,24]. This decreases the RC time constant of the device and increases the EO 3 dB bandwidth to more than 32 GHz, the Nyquist frequency of the 64 GBd data signal. This value was estimated by simulations and by measurements with similar devices. We may hence conclude that the signal quality in our transmission experiment was mainly limited by the 30 GHz drive amplifier, and not by the modulator itself.

#258670 Received 2 Feb 2016; revised 5 Mar 2016; accepted 11 Mar 2016; published 20 Apr 2016

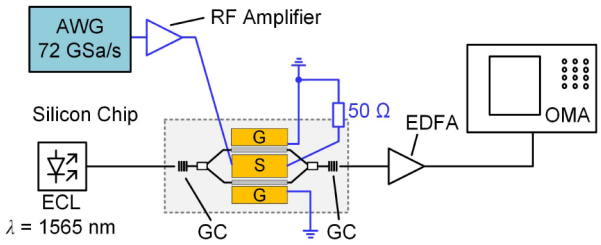

Fig. 2. Schematic of the experimental setup. Electrical multilevel drive signals at symbol rates of 36 GBd and 64 GBd are generated by an arbitrary waveform generator (AWG, Micram Instruments, AWG6020) with up to 72 GSa/s. The DC bias voltage for adjusting the operating point is applied to the MZM via a bias-T (not drawn), and the transmission line is terminated with 50 Ohm to avoid reflections. An external-cavity laser (ECL) at 1565 nm is used as an optical source and is coupled to the MZM chip via fibers and grating couplers. The optical output signal is amplified by an erbium-doped fiber amplifier (EDFA) and subsequently received by an optical modulation analyzer (OMA) in a homodyne configuration.

Without gate voltage, the EO bandwidth falls below 10 GHz. Optimized doping profiles allow to omit the gate voltage for future device generations, and we recently demonstrated an SOH device operating without gate voltage at 80 Gbit/s OOK [16]. For fabrication, we use a standard SOI wafer with a 220 nm thick device layer and a 3 µm thick BOX. The silicon waveguides are structured using electron beam lithography, while optical lithography is employed for defining the metallization. The chip is clad with the commercially available electro-optic material SEO100 from Soluxra, which is specified for operation at temperatures up to 85 °C [20]. The cladding material is poled by heating it close to its glass transition temperature of 140 °C while applying a poling voltage across the two floating ground electrodes of the MZM. Half of the voltage drops across each slot, resulting in an ordered orientation of the dipolar chromophores in the slot as indicated by the black arrows in Fig. 1(a). After cooling the device to room temperature, the orientation of the chromophores freezes and the poling voltage source is removed. The red arrows in Fig. 1(a) indicate the RF field applied to the GSG electrodes. It is antisymmetric with respect to the orientation of the chromophores, resulting in opposite phase shifts in the two arms of the MZM. Hence push-pull operation is achieved by connecting a single-ended data signal to the transmission line.

3. Experimental setup

The experimental setup for signal generation is sketched in Fig. 2. An arbitrary waveform generator (AWG, Micram Instruments model AWG6020) generates the electrical NRZ drive signal in form of a pseudo-random bit sequence with a length of 2^{11}–1. An electrical amplifier with 30 GHz bandwidth amplifies the signal to a peak-to-peak voltage of 2 V. This modulation voltage is coupled to the GSG transmission line via microwave probes. An external cavity laser (ECL) generates the optical carrier, which is coupled to the chip via grating couplers (GC). The optical output of the modulator is coupled to an erbium-doped fiber amplifier (EDFA) for compensating the excess loss of 21 dB which is dominated by the loss of the non-optimized grating couplers of 6 dB per facet. The MZM features an insertion loss of 9 dB, which is attributed to losses in passive components such as MMI and strip-to-slot converters (< 1 dB in total) [25], to propagation loss in the access waveguides caused by sidewall roughness (1 dB), and to free-carrier absorption [26] (≈ 1 dB) as well as scattering loss (6 dB) in the 750 µm long MZM slot waveguides. It is expected that these losses can be greatly reduced in future devices: Slot waveguides can be fabricated with propagation losses as low as 0.65 dB/mm [27], and optimizing the doping profile can reduce the doping-related losses to below 1 dB/mm. At the receiver side, an optical modulation analyzer (OMA) Agilent N4391A is used for homodyne detection and signal analysis. The OMA performs standard digital post-processing comprising polarization demultiplexing, phase estimation, and channel equalization. For signals with a symbol rate of 36 GBd the drive voltage at the input of the modulator is measured to be 2 V_{pp}.

#258670 Received 2 Feb 2016; revised 5 Mar 2016; accepted 11 Mar 2016; published 20 Apr 2016

For 64 GBd signals we use a linear electrical pre-emphasis to compensate low-pass characteristics of the setup, which are predominantly caused by the 30 GHz driver amplifier. The necessary pre-equalizer parameters are estimated at the receiver side and then applied to the AWG. Pre-equalization includes an increased voltage swing at the output of the AWG for compensating the low-pass roll-off. The resulting voltage level at the input of the modulator is estimated to remain at 2 V_{pp}. A constant gate field of 0.1 V/nm is applied between the silicon substrate and the device layer to improve the bandwidth of the device. The silicon chip with the SOH modulator is placed on a metallic sample holder which can be heated via a thermoelectric heater. The sample temperature is measured by a resistive temperature detector inside the sample holder and close to the silicon chip. Measurements are performed at room temperature as well as at 80 °C, without taking any measures to shield the devices from ambient oxygen. As modulation format, we use BPSK and 4ASK at symbol rates between 36 GBd and 64 GBd. Depending on the symbol rate, the AWG is operated at sampling rates of 72 GSa/s and 64 GSa/s, respectively.

4. Measurements

Measured eye patterns and constellation diagrams are shown in Fig. 3. The first set of measurements is performed at room temperature, upper row. For a second set, the sample is operated as before, but heated to 80 °C, lower row. After one hour at 80 °C in ambient atmosphere, we start the data recording. As a quantitative measure of the signal quality, we use the measured bit-error ratio (BER) and the error vector magnitude (EVM_m), which describes the effective distance of a received complex symbol from its ideal position in the constellation diagram, using the maximum length of an ideal constellation vector for normalization [28]. For operation of the device at 36 GBd, we find an average π-voltage of $U_\pi = 2.2$ V, estimated from the compression of the outer points in the 4ASK constellation diagrams. The corresponding voltage-length product at high-speed operation is therefore $U_\pi L = 1.6$ Vmm, which leads to an estimated EO coefficient of $r_{33} = 60$ pm/V. This $U_\pi L$ - product is slightly higher than the values measured for best-in-class devices [14,15], which we attribute to imperfect poling and to the fact that the material used in this work is not optimized only for highest EO activity but also for increased stability. There is vast potential in improving device performance by using cross-linkable materials with EO coefficients beyond 100 pm/V [29]. Nevertheless, even in the current experiment, the measured $U_\pi L$ - product is well below the 10 Vmm that are to be expected for conventional depletion-type devices [5].

For 36 GBd 4ASK signaling at room temperature, the EVM_m is measured to be 9.0%, and the BER is estimated to be approximately 1×10^{-5}. Too few errors were recorded for directly determining a statistically significant BER value. At 80 °C, the EVM_m increases slightly to 10.3%, and the BER is estimated to be 1×10^{-4}. The corresponding eye diagrams and the constellation diagrams are depicted in Fig. 3(a). For both temperatures, the BER are well below the threshold of 4.5×10^{-3} for hard-decision forward error correction (FEC) with 7% overhead [30]. At a symbol rate of 64 GBd we use a pre-emphasis to compensate for the low-pass characteristics in the measurement setup, which predominantly arise from the 30 GHz preamplifier (model SHF 807). The results for BPSK signaling at 64 GBd are shown in Fig. 3(b). The signal is error-free both for room temperature and for operation at 80 °C, i.e., no errors could be measured within our record length of 62.5 µs (8×10^6 bits). The EVM_m values of 17.1% and 19.0% indicate a BER smaller than 10^{-10} [28]. Figure 3(c) depicts the data for 64 GBd 4ASK signals. At room temperature, the measured EVM_m is 14.7% and the measured BER amounts to 4.3×10^{-3}, just below the threshold for hard-decision FEC. For operation at 80 °C, the EVM_m is measured to be 17.6%, and the measured BER is 1.3×10^{-2}, still below the threshold of 2.4×10^{-2} for soft-decision FEC with 20% overhead [31]. At room temperature, the line rate (net data rate) of the 64 GBd 4ASK signal amounts to 128 Gbit/s (120 Gbit/s). These figures represent the highest values demonstrated so far for a silicon-based Mach-Zehnder modulator.

#258670 Received 2 Feb 2016; revised 5 Mar 2016; accepted 11 Mar 2016; published 20 Apr 2016

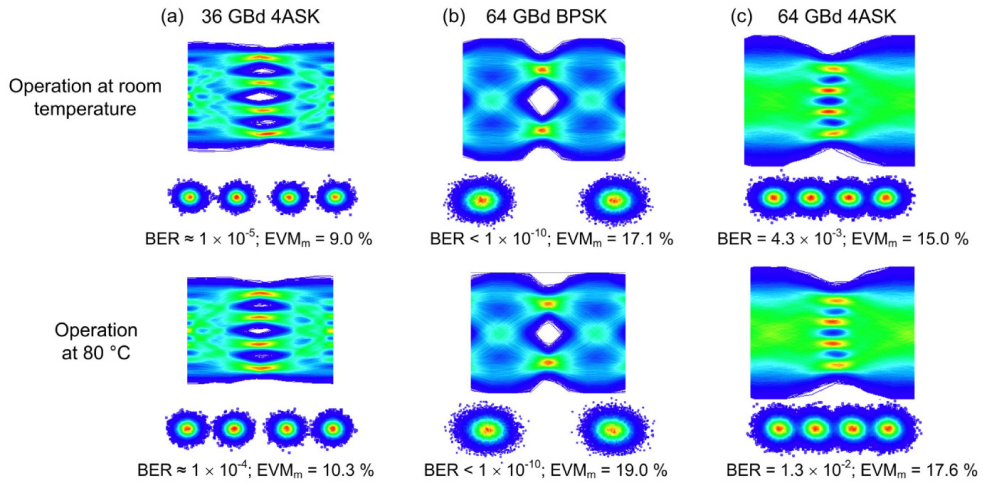

Fig. 3. Evaluation of the signal generation experiment. The top row depicts the measured eye diagrams and constellation diagrams for operation at room temperature. In the bottom row the corresponding data for operation at 80 °C is shown. (a) Signaling with 36 GBd 4ASK (72 Gbit/s) without pre-emphasis. At room temperature: $EVM_m = 9.0\%$, estimated BER is 1×10^{-5} (too few errors are measured within our record length of 62.5 µs for determining a reliable BER). At 80 °C: $EVM_m = 10.3\%$ is slightly increased, estimated BER is 1×10^{-4}. The peak-to-peak voltage at the modulator is measured to be 2 V_{pp}. (b) BPSK signaling at 64 GBd with pre-emphasis, error free performance (no errors measured in recording), both at room temperature and at 80 °C. The EVM_m indicates a BER $< 10^{-10}$. (c) 64 GBd 4ASK signaling (128 Gbit/s) with pre-emphasis. At room temperature: $EVM_m = 15.0\%$, BER $= 4.3 \times 10^{-3}$. At 80 °C: $EVM_m = 17.6\%$, BER $= 1.3 \times 10^{-2}$.

The slightly reduced signal quality at elevated temperatures is attributed to an increased π-voltage after burn-in. Using again the compression of the outer points in the 4ASK constellation diagrams to extract the π-voltage, we estimate a 12% increase as an upper limit for the degradation after burn-in. Apart from the burn-in phase, the performance of our modulator stayed constant over the entire measurement. Moreover, we did not observe any significant degradation of the devices over several months of repeated use and storage under normal laboratory conditions at room temperature. This is well in line with previous reports on the SEO100 material, where, after a short burn-in period, more than 90% of the material efficiency was retained for more than 500 hours [20]. These experiments provide a first proof-of-principle that SOH modulators can indeed be operated at elevated temperatures. A detailed investigation of aging and temperature stability of organic EO materials is subject to ongoing research. By using modified cross-linkable chromophores, the orientational stability of the chromophores can be further improved [32]. The viability of this approach has been demonstrated for EO compounds with high r_{33}, where material stability of up to 200 °C has been achieved [29,33].

5. Summary

We demonstrate the first high-speed operation of an SOH modulator at an elevated temperature of 80 °C in regular oxygen-rich ambient atmosphere. A single 750 µm long SOH Mach-Zehnder modulator is used to generate multilevel signals at symbol rates of up to 64 GBd. The achieved line rate of 128 Gbit/s and the corresponding net data rate of 120 Gbit/s correspond to the highest value demonstrated for a silicon-based Mach-Zehnder modulator so far. Based on these findings and on progress in EO material research, we expect that SOH modulators evolve towards high-performance devices with high reliability.

#258670 Received 2 Feb 2016; revised 5 Mar 2016; accepted 11 Mar 2016; published 20 Apr 2016

Acknowledgments

We acknowledge fruitful discussions with Larry Dalton at University of Washington. This work was supported by the European Research Council (ERC) Starting Grant 'EnTeraPIC', number 280145, by the Alfried Krupp von Bohlen und Halbach Foundation, by the EU-FP7 projects PhoxTroT and BigPipes, by the Helmholtz International Research School for Teratronics (HIRST), by the Karlsruhe School of Optics and Photonics (KSOP), by the Karlsruhe Nano-Micro Facility (KNMF) and by the Initiative and Networking Fund of the Helmholtz Association. We acknowledge support by Deutsche Forschungsgemeinschaft and Open Access Publishing Fund of Karlsruhe Institute of Technology.

#258670 Received 2 Feb 2016; revised 5 Mar 2016; accepted 11 Mar 2016; published 20 Apr 2016